JOURNAL OF MATERIALS SCIENCE 13 (1978) 825–832

Cavitation during superplastic flow of ternary alloys based on microduplex Pb-Sn eutectic

D. W. LIVESEY, N. RIDLEY
Department of Metallurgy, University of Manchester, Manchester, UK

The effect of phases having a range of hardnesses on the superplastic tensile behaviour of microduplex Pb–Sn eutectic has been studied. The presence of relatively hard particles induced cavitation at particle/matrix interfaces during deformation in an otherwise non-cavitating system, and the growth and interlinkage of cavities led to brittle superplastic fractures. Density measurements showed that cavitation increased as the volume fraction, hardness and size of intermetallic particles was increased. Increasing strain rate and decreasing deformation temperature also led to an increased level of cavitation. Cavity nucleation was attributed to the limited ability of the relatively hard phases to contribute to the accommodation processes occurring during superplastic flow.

1. Introduction

Superplastic deformation can lead to large strains, but there is evidence that a number of systems undergo cavitation during superplastic tensile straining, and this can restrict the elongation to fracture. Cavitation has been reported for Cu-base alloys [1–4], Fe-base alloys [5–7], Al-base alloys [8, 9], and for Zn–Al eutectoid [10].

Recently, Humphries and Ridley [11] have shown that cavitation can be induced in microduplex Pb–Sn eutectic during superplastic flow, by introducing the relatively hard intermetallic phase based on Ag_3Sn. The Pb–Sn eutectic was selected as a model system because its superplastic behaviour was well established, and also because there were no reports in the literature of cavitation occurring during superplastic flow. In the present work, the effect of a range of phases of different hardnesses based on Bi, SbSn, Ag_3Sn and Cu_6Sn_5 on superplastic behaviour and cavitation, has been examined by making additions of Bi, Sb, Ag or Cu to the Pb–Sn eutectic.

2. Materials

The Pb–Sn eutectic, the Pb–Sn–Bi ternary eutectic and several ternary alloys based on the Pb–Sn eutectic, were prepared from high purity metals (>99.9%) by induction melting in a graphite crucible in air. The alloy compositions are listed in Table I.

TABLE I Nominal and analysed compositions (wt %) of the alloys

Nominal composition	Analysed composition
Sn–38.1% Pb	
Sn–32.0% Pb–52% Bi	
Sn–36.6% Pb–4% Ag	4.09 ± 0.02% Ag
Sn–35.4% Pb–7% Ag	6.89 ± 0.02% Ag
Sn–36.6% Pb–4% Sb	4.13 ± 0.01% Sb
Sn–35.4% Pb–7% Sb	7.36 ± 0.01% Sb
Sn–36.6% Pb–4% Cu	4.30 ± 0.02% Cu

The alloys were chill cast into bars of 12 mm section weighing 150 to 200 g. The bars were then flat-rolled at room temperature to approximately 1.2 mm thickness, and tensile specimens of 10 mm gauge length and 5 mm gauge width were stamped out. All alloys, with the exception of Pb–Sn–Bi, were given an annealing treatment of 1 h at 100° C, to develop an equiaxed fine grain structure in accordance with previous work [11]. Recent work, by the authors, has shown that this annealing procedure is unnecessary.

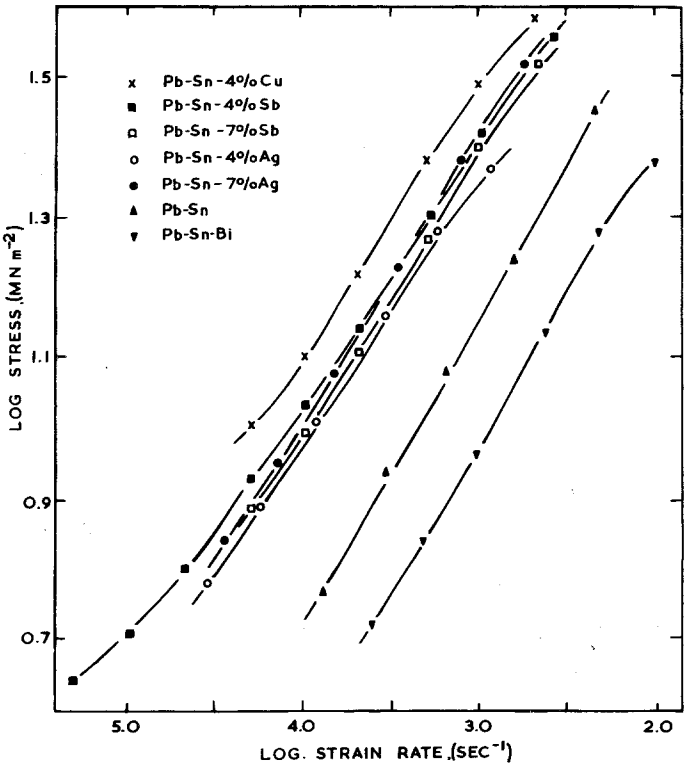

Figure 1 Logarithmic plots of stress versus strain rate for Pb–Sn based alloys at room temperature.

3. Experimental

Superplastic tensile straining was performed in air using an Instron machine. Most of the tests were made at room temperature, although a few elevated temperature tests were performed. Metallographic studies were made on surfaces prepared by an alternate polish and etch technique, which was used to remove any distorted surface layer. Final polishing was performed on γ-alumina, with 2% nital or 5% acid ferric chloride being used as etchants. Quantitative metallographic measurements of a number of microstructural features were made using a Quantimet 720 Image Analysing Computer (QTM).

Specimens, in both undeformed and superplastically strained conditions, were fractured in liquid nitrogen using a constant cross-head velocity of 8.33×10^{-3} mm sec^{-1}. This procedure was adopted to minimize plastic strain during fracture, and hence produce relatively flat fracture surfaces which were then examined in a Cambridge Stereoscan 180 SEM. The extent of cavitation resulting from superplastic deformation of specimens strained to pre-selected elongations, was measured by hydrostatic weighing in ethyl iodide. Differences in density between the gauge head and gauge length of a specimen were attributed to the presence of cavities in the gauge length.

A GKN microhardness tester was used to measure the hardness values of the phases present in the alloys. At least 10 indentations were made on each of the phases using a load of 3 g.

4. Results

4.1. Mechanical behaviour

Log stress–log strain rate curves were plotted for all the alloys at room temperature, and the results are summarized in Fig. 1. The Pb–Sn–Bi alloy has the usual sigmoidal-shaped curve involving low stress levels and a straight portion (stage II) consistent with superplastic flow. The Pb–Sn eutectic has higher flow stresses for the same strain rates. Addition of Sb or Ag (4% or 7%) increased the general stress level further, but there was no significant difference between any of these four stress–strain rate curves.

Addition of 4% Cu to the Pb–Sn eutectic displaced the curve to still higher stress levels. The strain rate sensitivity indices (m values), calculated from the maximum slope of the curves in Fig. 1, are given in Table II, together with the strain range over which the maximum slopes occurred. Values of m for all the alloys (excluding Pb–Sn–Bi) were very similar, and may be summarized as 0.425 ± 0.025. However, the superplastic behaviour was greatly influenced by the third element addition.

TABLE II Maximum values of strain rate sensitivity and corresponding strain rate range

Alloy	*m* value	Strain rate range ($sec^{-1} \times 10^4$)
Pb–Sn–Bi	0.48	5.3 to 53.3
Pb–Sn	0.45	1.5 to 4.6
Pb–Sn–4% Sb	0.41	2.2 to 11.0
Pb–Sn–7% Sb	0.40	1.2 to 11.0
Pb–Sn–4% Ag	0.42	0.8 to 8.3
Pb–Sn–7% Ag	0.40	0.7 to 6.0
Pb–Sn–4% Cu	0.43	2.2 to 5.3

The results of constant cross-head velocity to fracture tests on the ternary alloys are shown in Figs. 2 and 3. It can be seen that the elongation to fracture tends to go through a maximum with increasing initial strain rate. The maximum corresponds to an average strain rate at which maximum strain rate sensitivity occurs. Silhouettes of specimens of Pb–Sn–4% Cu fractured at elevated temperatures are shown in Fig. 4, and increasing temperature results in increasing elongation. Fig. 5 shows silhouettes of specimens of various compositions tested to failure at an initial strain rate of $1.66 \times 10^{-3}\ sec^{-1}$ and illustrates the effect that different alloy additions to Pb–Sn have on the cross-sectional area at fracture.

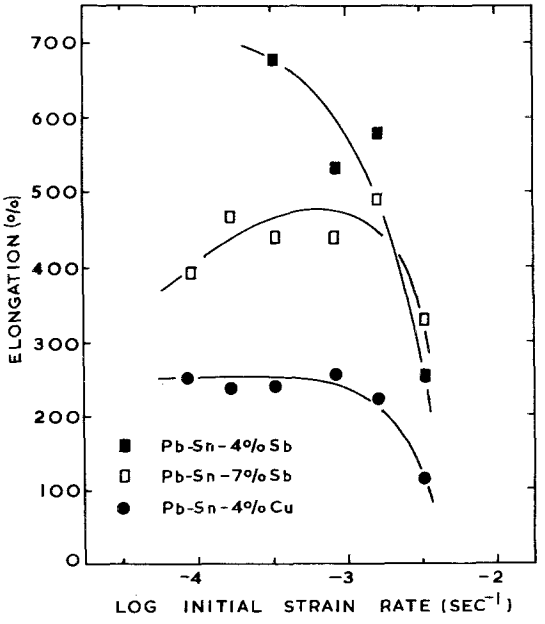

Figure 2 Effect of initial strain rate on elongation to fracture of Pb–Sn based alloys containing additions of antimony and copper.

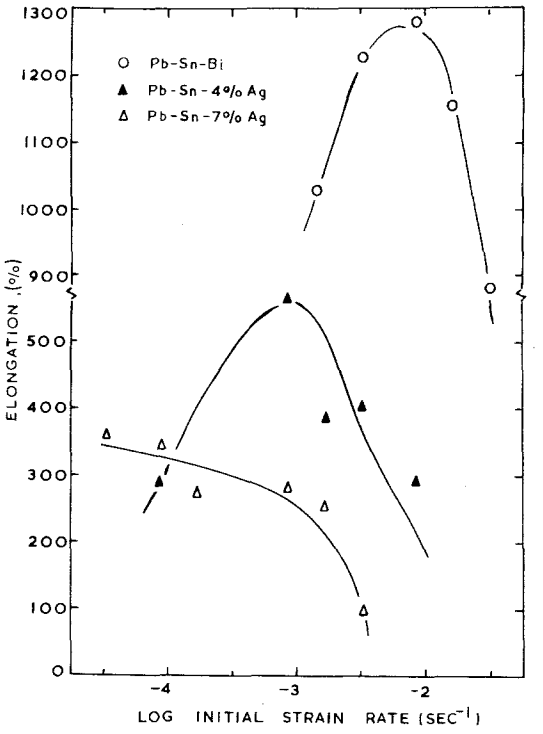

Figure 3 Effect of initial strain rate on elongation to fracture of Pb–Sn based alloys containing additions of bismuth and silver.

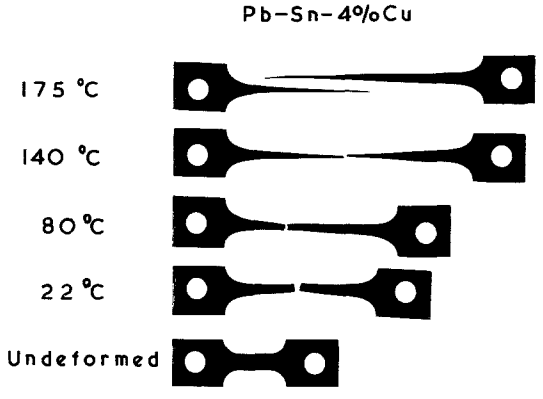

Figure 4 Silhouettes of Pb–Sn–4% Cu alloy strained to fracture at various temperatures.

4.2. Metallography

No positive identification of the crystal structures or compositions of the intermetallic compounds was made, as the main object of the additions was to produce phases with a range of hardness levels. Values of microhardness are recorded in Table III. Figs. 6a and b are optical micrographs and Fig. 7 is a scanning electron micrograph of longitudinal

sections of specimens pulled to 200% elongation at room temperature. White intermetallic particles are located in a microduplex matrix, similar to that observed in the Pb–Sn eutectic (dark phase Pb-rich, light phase Sn-rich). The micrographs show cuboids based on Sb–Sn in a specimen of Pb–Sn–7% Sb deformed at an initial strain rate of 1.66×10^{-3} sec^{-1} (Fig. 6a), irregularly shaped particles based on Cu_6Sn_5 in a specimen of Pb–Sn–4% Cu deformed at an initial strain rate of

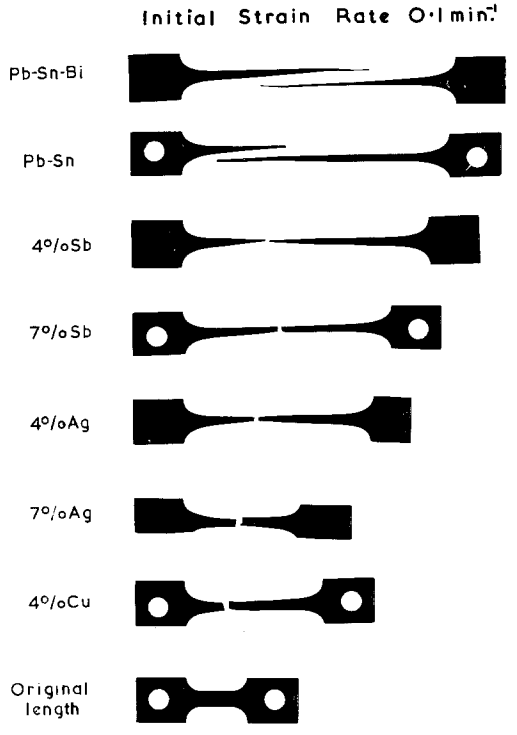

Figure 5 Silhouettes of Pb–Sn based alloys strained to fracture under the same conditions.

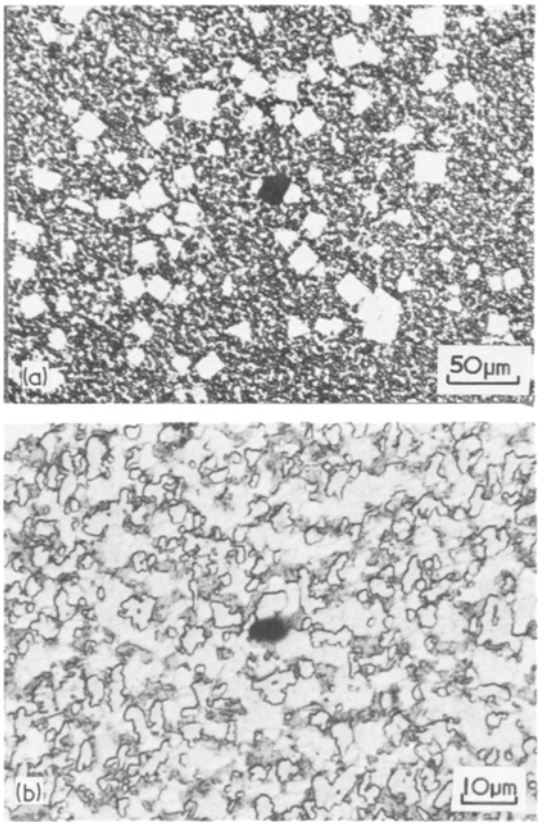

Figure 6 Optical micrographs of longitudinal sections of (a) Pb–Sn–7% Sb (b) Pb–Sn–4% Cu, strained to 200% elongation.

TABLE III Experimental data from quantitative metallography, microhardness testing and hydrostatic weighing

Addition	Phase based on:	Phase shape	% by volume
Bi	Bi solid solution	Cuboids	47.4
Sb (4% Sb)	SbSn (distorted cubic)	Irregular	5.4
Sb (7% Sb)		Cuboids	10.6
Ag (4% Ag)	Ag_3Sn (orthorhombic)	Irregular	6.2
Ag (7% Ag)		Irregular	9.5
Cu	Cu_6Sn_5 (hexagonal)	Irregular	6.1
Pb	Pb solid solution	Irregular	–
Sn	Sn solid solution	Irregular	–

Addition	Mean phase diameter (μm)	Microhardness (MNm^{-2})	Average cavitation (%)
Bi	1.5	69	0
Sb (4% Sb)	1.0	196	0.14
Sb (7% Sb)	11.0		0.69
Ag (4% Ag)	1.9	324	0.47
Ag (7% Ag)	1.7		0.95
Cu	2.3	726	0.81
Pb	2.2	20	–
Sn	–	29	–

1.66×10^{-4} sec^{-1} (Fig. 6b), and irregularly shaped particles based on Ag_3Sn in a specimen of Pb–Sn–7% Ag deformed at an initial strain rate of 8.33×10^{-4} sec^{-1} (Fig. 7). In each of the figures there is a clear association between intermetallic particles and cavities produced during superplastic deformation.

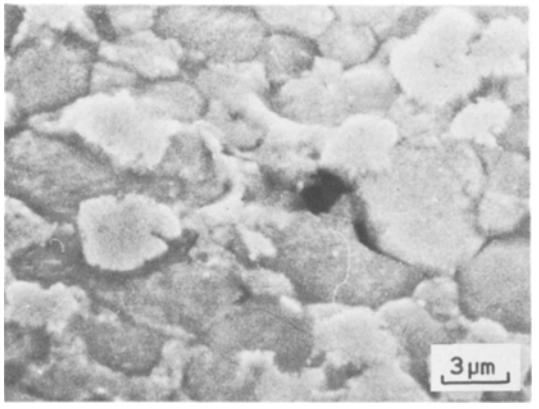

Figure 7 Scanning electron micrograph showing cavitation in superplastically deformed Pb–Sn–7% Ag alloy.

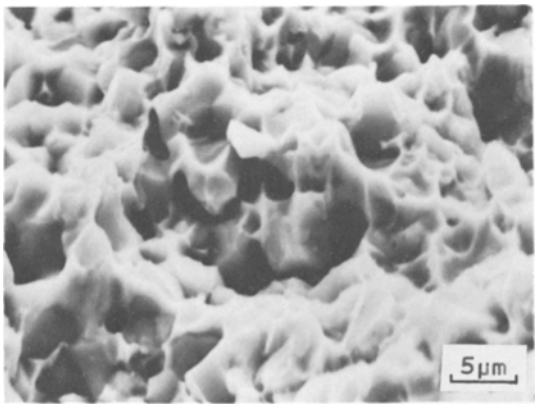

Figure 8 Pb–Sn–4% Cu alloy fractured in tension at −196° C showing pre-existing cavities.

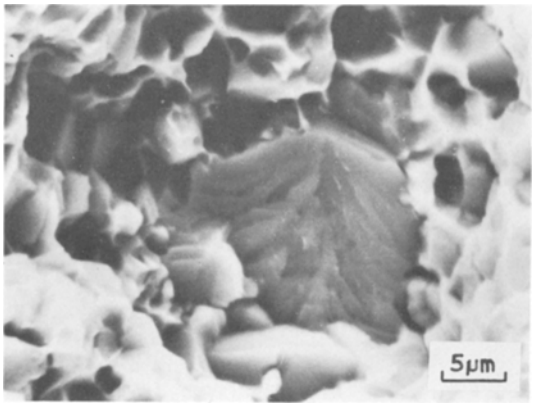

Figure 9 Shows SbSn cuboid associated with cavity in Pb–Sn–7% Sb alloy.

Further evidence of cavitation comes from fractography. Fig. 8 is a scanning electron micrograph of Pb–Sn–4% Cu, which had been deformed to 150% at an initial strain rate of 8.33×10^{-4} sec^{-1} at room temperature, and then broken in tension at −196° C. The mode of fracture is intergranular with ductile tearing. The fracture surface of a specimen of Pb–Sn–7% Sb, strained to 200% at initial strain rate of 8.33×10^{-4} sec^{-1}, is illustrated in Fig. 9. Large SbSn cuboids are associated with pre-existing voids.

All the experimental data from quantitative metallography has been summarized in Table III. Twenty different areas of each specimen were examined using the QTM and this involved an analysis of $\sim 10^7$ picture points. Errors associated with the measurements are related to lack of resolution between intermetallic particles and the Sn-rich matrix, and the limited number of size groups on the QTM. In addition, no correction procedure was used for sectioning errors (most particles being cut away from their position of maximum diameter). However, similar errors would occur for all alloys so that these measurements provide a basis for comparison.

4.3. Density

A quantitative assessment of the effect of strain rate on the level of cavitation was made for alloys

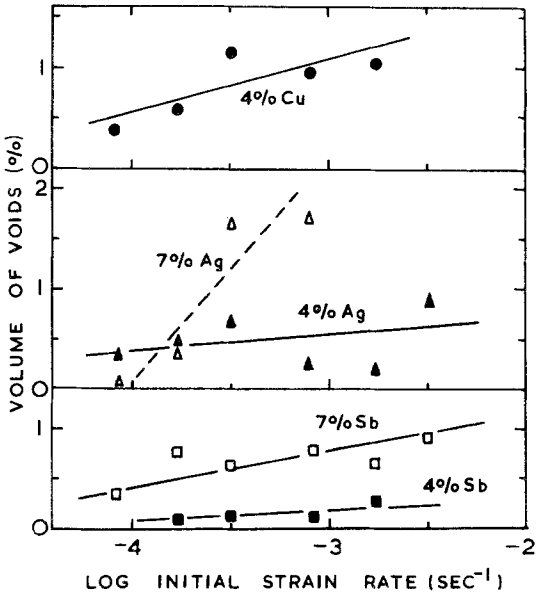

Figure 10 Volume of voids versus initial strain rate for Pb–Sn based alloys strained to 200% elongation.

deformed to 200% elongation at room temperature. Results are presented in Fig. 10, and an average value of cavitation over a range of initial strain rates, is also recorded in Table III for the purpose of comparing the different alloys. No cavitation could be detected in either Pb–Sn or Pb–Sn–Bi.

5. Discussion

5.1. Mechanical behaviour

Humphries and Ridley [11] have reported that the addition of Ag_3Sn to the microduplex Pb–Sn eutectic reduced both the m value and the elongation to fracture. In the present work, additions of 4% and 7% Ag were found to marginally decrease the m value. Similar observations were made for the other alloy additions, with the exception of bismuth, which appeared as a soft Bi-rich solid solution in the microstructure. Additions of Sb, Ag and Cu reduced the strain rate range of maximum strain rate sensitivity and displaced this range to lower values of strain rate.

True stress–true strain curves for Pb–Sn–4% Cu are plotted in Fig. 11 and have been calculated from load–elongation results, using assumptions of constant specimen volume and uniform deformation. At intermediate strain rates the Pb–Sn–4% Cu alloy showed a high resistance to necking, so the latter assumption was reasonable. The curves in Fig. 11 are influenced by several factors; strain rate (which decreases during the test), grain refinement or coarsening during the test, and also phase size and distribution changes which occur during deformation. At low strain rates there is an immediate strain hardening followed by an apparent strain softening, which accelerates towards the end of the test. Although the effect of increasing strain rate rotates the curves in a clockwise fashion, it may be deduced that, at low strain rates, a strain hardening effect from coarsening dominates. At higher strain rates a strain softening effect, arising from the removal of directionality produced by the prior rolling of the material, dominates. Metallography indicated that intermetallic particles tended to lie in bands in the rolling direction prior to deformation. Similar explanations to those above have been used by Suery and Baudelet [12], to explain the shape of true stress–true strain curves for a superplastic fibrous 60/40 brass.

Sagat and Taplin [2] have reported that a sudden increase in load bearing capacity occurs

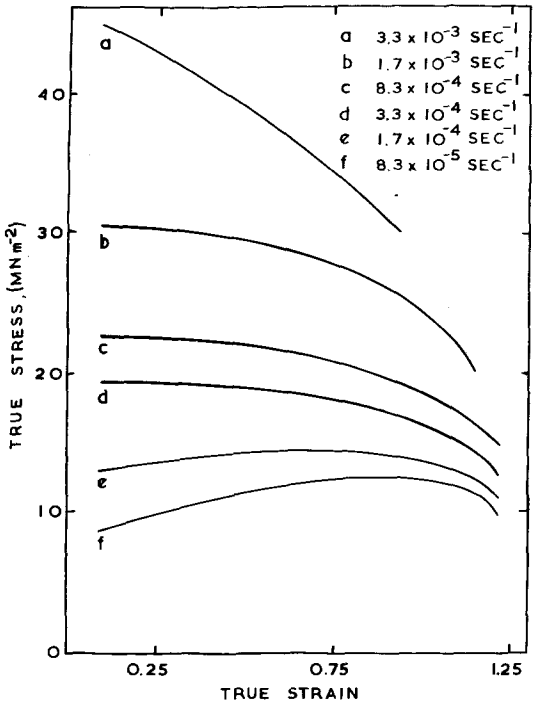

Figure 11 True stress–true strain curves for Pb–Sn–4% Cu superplastically deformed at different strain rates.

immediately prior to fracture during superplastic tensile straining of a ternary brass. This is caused by the formation of internal necks between cavities, which eventually deform in a non-superplastic manner and work harden. This appears to be a general phenomenon in cavitating Cu-base alloys, and has been recently observed in α/β nickel silvers by the authors. The absence of such a phenomenon in Fig. 11 suggests that the assumption of no external necking is invalid, but the relatively large cross-sectional area of the fracture surfaces of Pb–Sn–4% Cu would appear to contradict this view. An alternative explanation, is that the Pb and Sn-rich phases are able to deform superplastically at much higher strain rates than the phases involved in the copper-based alloys, with cavities remaining relatively discrete until close to the point of fracture.

5.2. Cavitation

In general, cavities will be nucleated whenever the rate of accommodation at triple points, grain-boundary irregularities etc. is exceeded by the rate of grain-boundary sliding. The incomplete accommodation results in stress concentrations which exceed the critical stress for cavity formation.

Accommodation at any potential nucleation

site will occur more readily if all the phases at this point can contribute to the accommodation process, whether this involves diffusion or dislocation glide. In the Pb–Sn and Pb–Sn–Bi eutectics accommodation can keep pace with the rate of grain-boundary sliding and there is no cavity nucleation. However, addition of elements which lead to the formation of intermetallic compounds results in cavitation, and metallographic examination shows that there is an association of cavities with the intermetallic particles. The level of cavitation increases with increasing volume fraction, size and hardness of intermetallic particles (Table III).

The increase in SbSn particle size as the antimony content in Pb–Sn–Sb is raised from 4% to 7% is quite marked. The reason for this is not understood, but the effect leads to the tentative conclusion that increase of particle size produces an increased level of cavitation. The number of particles per square micron (from QTM) for Pb–Sn–4% Sb is 0.037, while that for Pb–Sn–7% Sb is only 0.0036. Hence the number of potential nucleation sites in Pb–Sn–4% Sb is a factor of 10 greater than the number in Pb–Sn–7% Sb (as cavities are only associated with SbSn in both alloys). However, the level of cavitation in Pb–Sn–7% Sb is much higher than in the 4% Sb alloy. With increase of particle size there will be an increasing difficulty in obtaining complete accommodation by diffusion or dislocation means over the relatively large interfacial area between particles and matrix, because of greater geometrical restriction.

The effect of segregation of solute atoms, to the Pb-rich or Sn-rich phase boundaries, on surface energy is unlikely to be of sufficient magnitude to permit cavity nucleation at matrix phase boundaries. However, once cavities are nucleated at the intermetallic particles then growth can occur along matrix boundaries. In the SEM micrograph (Fig. 7) of Pb–Sn–7% Ag, a cavity seems to be growing along a particle/matrix boundary.

The alloy addition performs two functions which aid nucleation of cavities. Firstly, the general flow stress is raised and secondly, particles which act as sites for cavity formation are introduced into the microstructure. However, it is unlikely that cavity nucleation would occur in the absence of hard particles, since the flow stress of the binary alloy may be raised by increasing the strain rate without cavitation taking place.

The Pb–Sn–7% Sb alloy has striking similarities with microduplex stainless steels [5]. Fig. 9 is similar to micrographs showing Ti(C, N) inclusions located in pre-existing voids in stainless steels, which were superplastically deformed and then fractured in tension at room temperature. In the case of the steels, it was clear that some of the cavities developed from cracks in the particles which were probably caused by prior mechanical processing. There was little metallographic evidence to suggest cracking of intermetallics or matrix/particle decohesion made a significant contribution to cavitation in the present alloys. However, during examination of the fracture surfaces of non-superplastically deformed Pb–Sn–4% Cu, internal cracks were occasionally observed and these could have been produced by prior rolling of the material.

The relationship between degree of cavitation and particle hardness has been demonstrated. Increase of particle hardness implies an increasing contribution of covalent or ionic bonding in the intermetallic compound, and hence an increasing difficulty of accommodation by dislocation or diffusional means within the phase and in addition, a decreasing coherency between particles and matrix. All the above factors will tend to promote void nucleation. Fig. 10 indicates there is considerable scatter in the results, which could be due to the difficulty of obtaining a uniform distribution of hard particles. However, it is reasonable to expect that the higher stress levels involved at faster strain rates will make it more probable that a given particle will nucleate a cavity.

Limited studies on specimens of Pb–Sn–4% Cu, deformed at elevated temperature, have shown that cavitation decreases rapidly with increasing temperature. The area of fracture surface diminishes with increasing temperature, as can be seen in Fig. 4, and this is consistent with a decrease in the level of cavitation. The large temperature dependence of flow stress could result in local stress concentrations at potential nucleation sites falling below the threshold for cavity nucleation, at higher temperatures. At the relatively low temperatures involved this is more likely to be due to increased accommodation in the Pb–Sn matrix rather than in the intermetallic phase.

6. Conclusions

(1) The introduction of hard particles into micro-duplex Pb–Sn eutectic reduced the superplasticity of the material as measured by tensile elongation to fracture, while the relatively soft Bi-rich solid solution produced the opposite effect.

(2) The presence of hard intermetallic phases caused cavitation to occur in the normally non-cavitating Pb–Sn eutectic.

(3) Cavities were found to be associated with intermetallic phase matrix interfaces.

(4) The level of cavitation increased as the volume fraction, hardness and size of the intermetallic phase particles was increased. An increase in strain rate, or decrease in deformation temperature, also resulted in an increased level of cavitation.

(5) Cavitation was attributed to incomplete accommodation at the interfaces due to restricted accommodation within the intermetallic phase.

Acknowledgement

One of the authors (DWL) is grateful to the Science Research Council for the award of a Research Studentship.

References

1. S. SAGAT, P. BLENKINSOP and D. M. R. TAPLIN, *J. Inst. Metals* **100** (1972) 268.
2. S. SAGAT and D. M. R. TAPLIN, *Acta Met.* **24** (1976) 307.
3. D. M. R. TAPLIN, G. L. DUNLOP, S. SAGAT and R. H. JOHNSON, Proceedings of the II Inter-American Conference on Materials Technology, Mexico City (ASME, New York, 1970) p. 1253.
4. N. RIDLEY, C. W. HUMPHRIES and D. W. LIVESEY, Proceedings of the 4th International Conference on the Strength of Metals and Alloys, (E.N.S.M.I.M., Nancy, 1976) p. 433.
5. W. B. MORRISON, *ASM Trans. Quart.* **61** (1968) 423.
6. C. W. HUMPHRIES and N. RIDLEY. *J. Mater Sci.* **9** (1974) 191.
7. C. I. SMITH and N. RIDLEY. *Metals Technology* **1** (1974) 191.
8. K. MATUKI and M. YAMODA, *J. Japan. Inst. Metals* **37** (1973) 448.
9. D. M. R. TAPLIN and R. F. SMITH, "Fracture 1977", Vol. 2, Edited by D. M. R. Taplin (University of Waterloo Press, Waterloo, 1977) p. 337.
10. H. ISHIKAWA, D. G. BHAT, F. A. MOHAMED and T. G. LANGDON, *Met. Trans.* **8A** (1977) 524.
11. C. W. HUMPHRIES and N. RIDLEY. *J. Mater. Sci.* **12** (1977) 851.
12. M. SUERY and B. BAUDELET, *ibid* **8** (1973) 363.

Received 10 June and accepted 22 July 1977.